

State-to-state endothermic and nearly thermoneutral reactions in an ultracold atom-dimer mixture

Jun Rui,* Huan Yang,* Lan Liu, De-Chao Zhang, Ya-Xiong Liu, Jue Nan, Bo Zhao, and Jian-Wei Pan
*Shanghai Branch, National Laboratory for Physical Sciences at Microscale and Department of Modern Physics,
University of Science and Technology of China, Hefei, Anhui 230026, China*
*CAS Center for Excellence and Synergetic Innovation Center in Quantum Information and Quantum Physics,
University of Science and Technology of China, Shanghai 201315, China and
CAS-Alibaba Quantum Computing Laboratory, Shanghai 201315, China*

Chemical reactions at ultracold temperature provide an ideal platform to study chemical reactivity at the fundamental level, and to understand how chemical reactions are governed by quantum mechanics [1–4]. Recent years have witnessed the remarkable progress in studying ultracold chemistry with ultracold molecules [5–15]. However, these works were limited to exothermic reactions. The direct observation of state-to-state ultracold endothermic reaction remains elusive. Here we report on the investigation of endothermic and nearly thermoneutral atom-exchange reactions in an ultracold atom-dimer mixture. By developing an indirect reactant-preparation method based on a molecular bound-bound transition, we are able to directly observe a universal endothermic reaction with tunable energy threshold and study the state-to-state reaction dynamics. The reaction rate coefficients show a strikingly threshold phenomenon. The influence of the reverse reaction on the reaction dynamics is observed for the endothermic and nearly thermoneutral reactions. We carry out zero-range quantum mechanical scattering calculations to obtain the reaction rate coefficients, and the three-body parameter is determined by comparison with the experiments. The observed endothermic and nearly thermoneutral reaction may be employed to implement collisional Sisyphus cooling of molecules [16], study the chemical reactions in degenerate quantum gases [17, 18] and conduct quantum simulation of Kondo effect with ultracold atoms [19, 20].

Ultracold molecules represent great opportunities to explore cold controlled chemistry and study state-to-state reaction dynamics at the quantum level [2, 17, 21]. Recently, with the development of ultracold molecule techniques, significant progress has been achieved in studying ultracold bimolecular reactions. Molecule-molecule [9–11] and atom-dimer [12–14] atom-exchange reactions have been observed at temperatures below 1 μ K. However, these studies are limited to exothermic

reactions, and ultracold reactions in the endothermic regime remain unexplored. Endothermic reactions are qualitatively different from exothermic reactions due to the presence of energy thresholds. Therefore ultracold endothermic reactions are expected to show threshold phenomenon, i.e., the reaction rate coefficients decrease remarkably when the threshold is changed from zero to a small positive value. Further, for ultracold endothermic reactions, the kinetic energy converts into internal energy and thus the resultant products are colder than reactants, which means that both the reactants and products should be described by quantum mechanics. This is in contrast to most of ultracold exothermic reactions where only the reactants are cold, whereas the products are much hotter due to the large exothermicity, and consequently the products can still be described by classical treatment [22].

Exothermic reactions in ultracold gases always lead to detrimental effects, such as loss of the molecules or heating of the samples, and thus they are expected to be suppressed [4]. In contrast, endothermic reactions do not cause heating and may even result in cold products. It has been proposed that endothermic inelastic collision may be employed to implement collisional Sisyphus cooling of molecules [16]. Moreover, endothermic reactions may offer a platform to study superchemistry where quantum degeneracy may strongly affect the reaction [17, 18], since they will not destroy quantum degeneracy due to heating. Besides, the thermoneutral reaction (zero energy change, neither exothermic nor endothermic) may be employed to implement quantum simulation of the Kondo effect with ultracold atoms, as proposed in reference [19].

Exploring endothermic reactions at nearly zero temperature are challenging, because the collision energies of the reactants are much smaller than the threshold of most of endothermic reactions and thus the reaction should be simply forbidden. Theoretical schemes have been proposed to use laser to control an isotope-exchange reaction to be endothermic [23]. These techniques remain to be demonstrated. So far, the universal atom-exchange reactions with weakly bound Feshbach molecules [12–14] offer a unique possibility to study the endothermic reaction at nearly zero temperature. The reaction can be tuned to be exothermic, endothermic, or thermoneutral by simply varying the magnetic field.

*These authors contributed equally to this work.

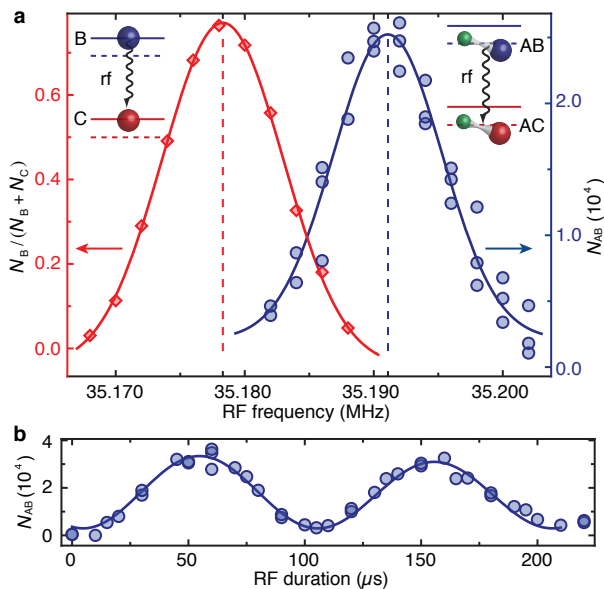


FIG. 1: **Molecular bound-bound rf spectrum and Rabi oscillation.** **a**, The measured atomic transition spectrum (red diamonds) and molecular bound-bound spectrum (blue circles) at 130.29 G. For the atomic spectrum, the fraction of the B atoms is recorded. For the molecular spectrum, the number of molecules transferred into the AB state is recorded by imaging the dissociated K atoms in the $|9/2, -7/2\rangle$ state. The data points are fitted with Gaussian functions. **b**, The measured bound-bound Rabi oscillation between the AB and AC molecule states at 130.26 G. The bound-bound Rabi frequency is fitted to be $2\pi \times 9.9(1)$ kHz.

Despite the easy tunability of the energetics, the direct observation of the state-to-state universal endothermic reactions and measurement of the reaction rate remain unsolved questions. In Refs. [12, 13], only the overall loss rates of the molecule reactants are observed. Although in Ref. [12] it is claimed that a pronounced threshold behaviour is observed in the endothermic regime, the observed overall loss rate includes the contribution from both the endothermic exchange reaction and the exothermic vibrational relaxation into deeply bound states, and the theoretical model has shown that dominant loss mechanism is actually the exothermic vibrational relaxation. In Ref. [14], the state-to-state reaction rate can only be measured in the exothermic regime with large released energy.

Here we report on the study of the state-to-state endothermic and nearly thermoneutral reaction in an ultracold atom-dimer mixture. Our experiment starts with approximately 3.0×10^5 ^{23}Na atoms and 1.6×10^5 ^{40}K atoms at about 600 nK in a crossed-beam optical dipole trap. The measured trap frequencies for K are $h \times (250, 237, 79)$ Hz, with h being the Planck constant. The Na atoms are prepared in the lowest hyperfine $|F, m_F\rangle_{\text{Na}} = |1, 1\rangle$ state, and the K atoms can be prepared in any hyperfine ground state $|F, m_F\rangle_{\text{K}} = |9/2, -9/2\rangle \dots |9/2, 9/2\rangle$.

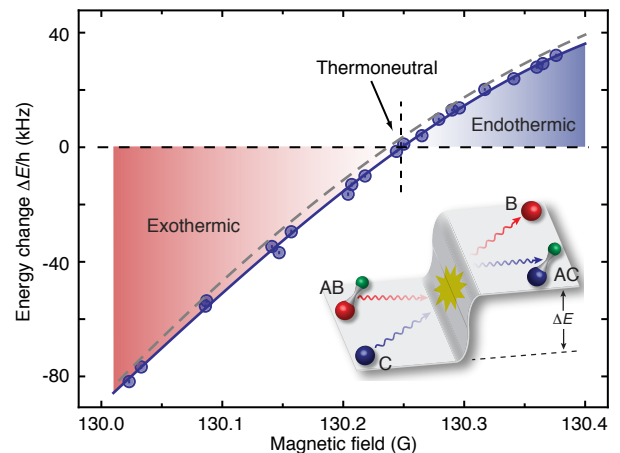


FIG. 2: **The reaction energy changes versus magnetic field.** The measured energy change ΔE for the reaction $\text{AB} + \text{C} \rightarrow \text{AC} + \text{B}$ as a function of the magnetic field. The energy change is precisely determined by measuring the molecular bound-bound transition frequency and the free atom-atom transition frequency using rf spectroscopy. The blue solid line is a polynomial fit to the data points. The vertical dashed line marks the magnetic field $B_{\text{tn}} = 130.249(2)$ G at which the reaction is thermoneutral with zero energy change. For $B < B_{\text{tn}}$ the reaction is exothermic, and for $B > B_{\text{tn}}$ the reaction is endothermic. As a comparison, the grey dashed line shows the energy change obtained from the difference between the two binding energy curves. Error bars inside the circles represent ± 1 s.d.

At a magnetic field near 130 G, the interspecies Feshbach resonance between $|1, 1\rangle$ and $|9/2, -3/2\rangle$ and the Feshbach resonance between $|1, 1\rangle$ and $|9/2, -5/2\rangle$ overlap (Supplementary Information). The overlapping Feshbach resonances allow studying the universal atom-exchange reaction between weakly bound Feshbach molecules and atoms [12–14, 24]. In our experiment, the reaction may be described by $\text{AB} + \text{C} \rightarrow \text{AC} + \text{B}$, where A denotes ^{23}Na atom in the $|1, 1\rangle$ state, and B and C denote ^{40}K atoms in the $|9/2, -5/2\rangle$ and $|9/2, -3/2\rangle$ state respectively. The AB and AC molecules are the corresponding NaK Feshbach molecules with binding energies E_{AB}^{b} and E_{AC}^{b} , respectively. The energy change in the reaction is given by $\Delta E = E_{\text{AB}}^{\text{b}} - E_{\text{AC}}^{\text{b}}$. The state-to-state reaction dynamics can be measured by preparing the reactant mixture and then monitoring the time evolution of AB reactant and B product, and the reaction rate coefficient is extracted from the time evolution. For detection, the AB molecules are dissociated into the $\text{A} + |9/2, -7/2\rangle$ state and the B atoms are transferred to the $|9/2, -7/2\rangle$ state by rf pulses, and the AB molecule number and B atom number are determined by measuring the atom number in the $|9/2, -7/2\rangle$ state, respectively.

In all previous works studying ultracold reaction with Feshbach molecules, the molecule reactants are directly formed using magnetic field association [12, 13] or radio frequency association [14]. However, these methods

cannot measure the reaction rate in the endothermic regime, either due to the low formation efficiency or large background noise caused by the preparation process.

In our system, the primary experimental challenge is to efficiently prepare the reactants $AB + C$ at the magnetic fields where endothermic reactions with small ΔE may occur. For the exothermic reactions with large and negative ΔE , the reactants can be prepared by radio frequency (rf) association [14, 25] of the AB molecule from an $A + C$ mixture. However, this preparation method is not applicable for small $|\Delta E|$, because in this regime the scattering lengths a_{AB} and a_{AC} in the two scattering channels are close to each other. This results in a rather low association efficiency since the bound-free Franck-Condon factor $F_{bf} \propto (1 - a_{AC}/a_{AB})^2$ is largely suppressed [26].

To circumvent this problem, we develop an indirect reactant-preparation method based on the molecular bound-bound transition. Instead of directly forming the AB molecules, we first associate the AC molecules from the $A + |9/2, -1/2\rangle$ mixture and then transfer the weakly bound molecules from the AC to the AB state by an rf π pulse. A subsequent rf π pulse transferring the free K atoms from the $|9/2, -1/2\rangle$ state to the C state then prepares the desired reactants. The idea behind this method is that for a small $|\Delta E|$, the suppression of bound-free Franck-Condon factor is accompanied by an enhancement of the bound-bound Franck-Condon factor [26] $F_{bb} \propto 4a_{AC}a_{AB}/(a_{AC} + a_{AB})^2$. Therefore, although it is difficult to form the AB molecule from the $A + C$ scattering state, it does allow us to create the AB molecule from the AC bound state.

The Feshbach resonance between the A and C atoms tends to be closed-channel dominated, and thus the AC molecules can only be efficiently associated when close to the resonance. In our experiment, we can efficiently form the AC molecules in a small magnetic field window between 130.02 G and 130.38 G using Raman photoassociation (Supplementary Information). The bound-bound rf spectrum and Rabi oscillation are measured, as shown in Fig. 1. The difference between the bound-bound transition frequency and the free-free transition frequency precisely determines the energy change $\Delta E = h(\nu_{AC \rightarrow AB} - \nu_{C \rightarrow B})$ of the reaction, which is in the range $h \times (-82, 32)$ kHz. The measured ΔE as a function of the magnetic field is shown in Fig. 2. The polynomial fit yields $\Delta E = 0$ at $B_{tn} = 130.249(2)$ G, which agrees well with the value of 130.24(1) G determined from the intersection point of the binding energy curves. The bound-bound transition has an efficiency of better than 95%, thanks to the enhanced bound-bound Franck-Condon factor, and approximately 2×10^4 AB molecules are formed. After preparing the reactants, the time evolutions of the AB molecule reactants and the B atom products are recorded.

The reaction dynamics are shown in Fig. 3. For magnetic fields larger than B_{tn} , the reaction is endothermic with $\Delta E > 0$. With increasing magnetic

field the reaction threshold increases and the maximum number of the B products decreases quickly. Using the indirect preparation method, the endothermic reaction is clearly observed up to 130.38 G with a reaction threshold of 32 kHz.

At 130.25 G, the observed reaction is a nearly thermoneutral reaction with the measured energy change $\Delta E = h \times 1.1(2)$ kHz. The ideal thermoneutral reaction has zero energy change [27], i.e., $\Delta E = 0$. Previously, the thermoneutral reaction usually refers to the “reaction” that the reactants and products are identical, e.g., $H_2 + H \rightarrow H_2 + H$, where H_2 and H are the hydrogen molecule and atom in their lowest internal states, respectively [1]. However, this is not an observable reaction. In our system, by preparing the reactants at the magnetic field where the Feshbach molecules have exactly the same binding energy, an observable thermoneutral reaction can be realized. In the current experiment, the achievable minimal energy change is limited by the resolution and uncertainty of the magnetic field.

We analyze the data by fitting the time evolution of the AB reactant and B product numbers using exponentials. As shown in Fig. 3a, we find that for the exothermic reactions, the two $1/e$ time constants τ_{AB} and τ_B agree with each other within mutual uncertainties, whereas for the endothermic reactions and nearly thermoneutral reactions, the two time constants are different from each other. We attribute this discrepancy to the influence of the reverse reaction $AC + B \rightarrow AB + C$, i.e., the reaction is reversible.

To demonstrate that this discrepancy is caused by the reverse reaction, we continuously remove the AC molecule products from the reaction mixture by dissociating them into the $A + |9/2, -1/2\rangle$ state. To do so, we first remove the A atoms after the AB molecules have been prepared. Then during the reaction process, we use the Raman light to continuously dissociate the AC molecules into the $A + |9/2, -1/2\rangle$ state (see Supplementary Information). This procedure suppresses the reverse reaction and makes the reaction irreversible. In this way, we find τ_{AB} and τ_B agree with each other within mutual uncertainties also for the endothermic and nearly thermoneutral reactions, as shown in Fig. 3b.

We now estimate the reaction rate coefficient β_r from the measured time evolutions. Taking the reverse reaction into account, the time evolution of the number of B products may be described by

$$\dot{N}_B = \beta_r \bar{n}_C N_{AB} - k_{re} N_{AC} N_B, \quad (1)$$

where the first and second terms on the right side of Eq. (1) account for the forward and reverse reactions, respectively. By continuously removing the AC products, the second term can be safely neglected. The mean density of the C atoms is approximated by $\bar{n}_C = \alpha N_C$, with $\alpha = ((m_K \bar{\omega}^2)/(4\pi k_B T))^{3/2}$, where $\bar{\omega}$ and T are the geometric mean of the trap frequencies and the temperature, respectively. We have assumed \bar{n}_C to be a constant as the number of the AB molecules is about

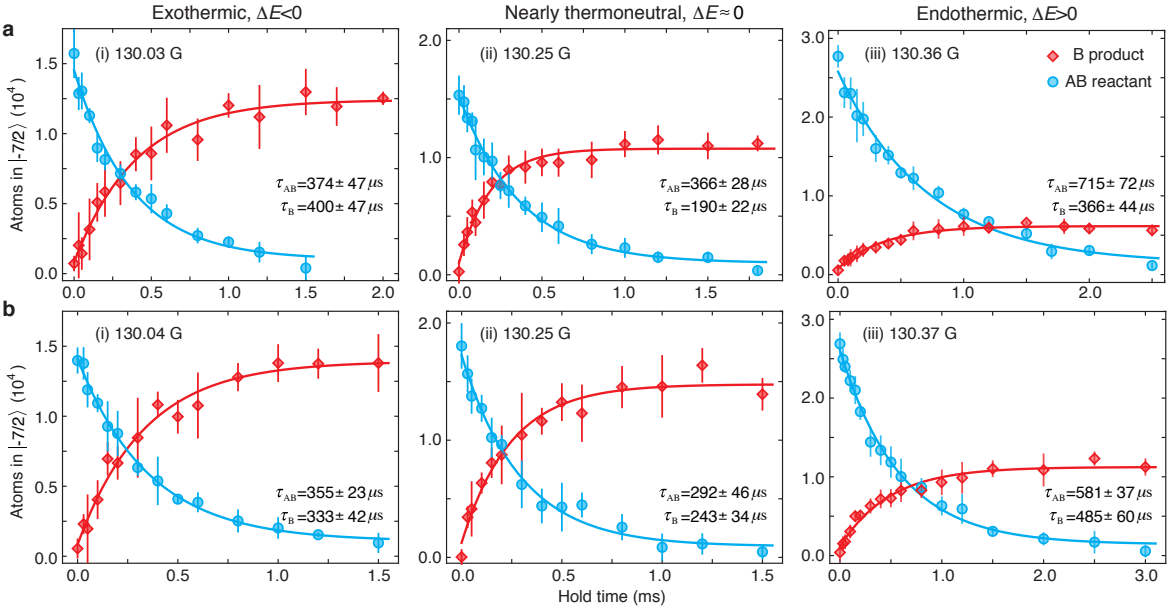


FIG. 3: **The reaction dynamics.** **a**, The decay of the AB reactant (blue circles) and the increase of the B product (red diamonds) as a function of the hold time, for (i) the exothermic reaction at $B = 130.03$ G with $\Delta E = -76.7(3)$ kHz, (ii) the nearly thermoneutral reaction at $B = 130.25$ G with $\Delta E = 1.1(2)$ kHz, and (iii) the endothermic reaction at $B = 130.36$ G with $\Delta E = 28.0(2)$ kHz. The blue and red solid lines are exponential fitting curves with $1/e$ time constants τ_{AB} and τ_B , respectively. For the exothermic reaction, τ_{AB} and τ_B agree with each other within mutual uncertainties, whereas for the endothermic and nearly thermoneutral reactions, τ_{AB} and τ_B are not consistent. **b**, The time evolution of the AB reactant (blue circles) and the B product (red diamonds) after continuously removing the AC product in the reaction process. The two time constants τ_{AB} and τ_B are consistent with each other within the mutual uncertainties also for the endothermic and nearly thermoneutral reactions, and the increased numbers of the B products are larger. Error bars represent ± 1 s.d.

one order of magnitude smaller than the number of the C atoms. The reverse reaction complicates the reaction dynamics, but the reaction rate coefficient may still be extracted using the simple equation

$$\beta_r = \frac{\dot{N}_B(0)}{\bar{n}_C N_{AB}(0)}, \quad (2)$$

where $N_{AB}(0)$ is the initial number of the AB molecules and $\dot{N}_B(0)$ is the initial derivative of the time evolution of the B atoms. Eq. (2) is also applicable to the reversible reaction, since we start from the $AB + C$ mixture and thus at $t = 0$ the products N_{AC} and N_B are both negligible. We assume that $N_{AB}(t)$ and $\dot{N}_B(t)$ can be approximated by exponentials, and obtain $\dot{N}_B(0)$ and $N_{AB}(0)$ from exponential fits of the measured data points. As shown in Fig. 4, the reaction rate coefficients obtained in this way are similar to the results in the case where the reverse reaction has been suppressed.

For the exothermic reactions, the reaction rate coefficient increases as the magnetic field increases. This may be qualitatively understood from the increase of the overlap between the wave functions of the two weakly bound molecules, when the difference between the two scattering lengths decreases [12, 24]. For the endothermic reaction, the reaction rate coefficient shows a strikingly threshold behaviour, as expected. Besides, the ratio

between the increased number of the B products and the initial number of the AB reactants is given in the inset of Fig. 4. The data points after removing the A atoms and the AC molecules directly give the branching ratio of the reaction.

To understand the reaction rate, we perform quantum mechanical reactive scattering calculations using the zero-range approximation. This is justified since in our experiments the scattering lengths a_{AB} and a_{AC} are both much larger than the van der Waals lengths, and the binding energies of the AB and AC molecules are well described by the universal model (Supplementary Information). In this case, the s -wave atom-dimer scattering may be described by the generalized Skorniakov-Ter-Martirosian (STM) equations [28–30]. In the STM equations, the only input parameters are the scattering lengths a_{AB} and a_{AC} (Supplementary Information), and the unknown three-body parameter Λ , which will be determined by comparing the reaction rates.

By numerically solving the STM equations, we calculate the reaction rate coefficients with Λ being a fitting parameter. The results are compared with the experiment for the magnetic fields between 129.44 G and 130.38 G, where the data points for exothermic reactions between 129.44 G and 129.91 G are obtained from our previous work [14]. We find that for a range of

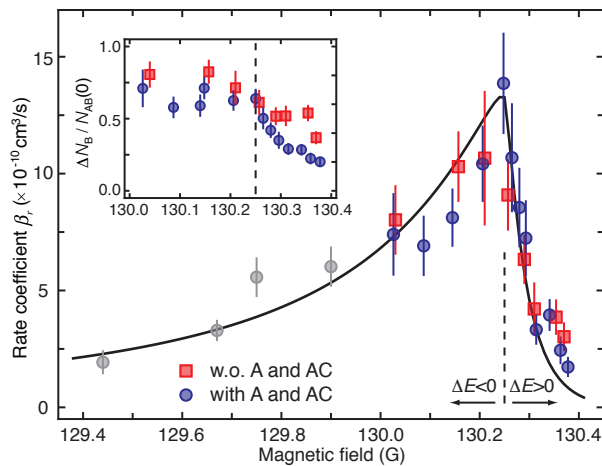


FIG. 4: **The behaviour of the reaction rate coefficients as a function of the magnetic field.** The blue circles and red squares represent the data points measured by using the indirect reactant-preparation method. The red squares are the data points obtained by continuously removing the AC molecules (after eliminating the A atoms) when the reverse reactions are significantly suppressed. The grey circles represent the data points obtained from Ref. [14]. The solid line is the numerical result with the fitted three-body parameter $\Lambda = 22.6/a_0$ and the normalization coefficient $C_\beta = 1.4$. The inset shows the ratios between the net increase of the B atom product and the initial AB molecule number, where the square points give the reaction branching ratio. Error bars represent ± 1 s.d.

values for Λ , the shapes of the theoretical curves and the experimental data points qualitatively agree with each

other, whereas the measured rate coefficients are larger than the calculated ones. We attribute this discrepancy to the systematic shifts in our data due to uncertainties in the particle numbers, density calibration and so on. Therefore, we include a normalization factor C_β as the second fitting parameter. As shown in Fig. 4, we find good agreement between the theory and the experiment with the fitting parameters $\Lambda = 22.6/a_0$ and $C_\beta = 1.4$, where a_0 is the Bohr radius.

In conclusion, we have experimentally studied state-to-state endothermic and nearly thermoneutral reactions in an ultracold atom-dimer mixture. The universal character of the reaction allows us to understand the reaction from a zero-range quantum mechanical scattering calculation. The study of endothermic reaction opens up the realistic avenue to implement collisional Sisyphus cooling of molecules [16]. The observation of thermoneutral reaction is crucial to the quantum simulation of the Kondo effect with ultracold molecules [19, 20]. This scheme requires the Feshbach molecules to have almost the same binding energy [19], which is exactly the nearly thermoneutral regime demonstrated in our work.

We would like to thank Peng Zhang, Cheng Chin, and Matthias Weidemüller for helpful discussions, and Hui Wang, Xing Ding and Xiao-Tian Xu for their important assistances. We acknowledge Ingo Nosske for carefully reading the manuscript. This work was supported by the National Natural Science Foundation of China (under Grant No.11521063, 11274292), the National Fundamental Research Program (under Grant No. 2013CB336800), and the Chinese Academy of Sciences.

-
- [1] Stwalley, W. C. Collisions and reactions of ultracold molecules. *Can. J. Chem* **82**, 709 (2004).
- [2] Krems, R. V. Cold controlled chemistry. *Phys. Chem. Chem. Phys.* **10**, 4079 (2008).
- [3] Bell, M. T. & Softley, T. P. Ultracold molecules and ultracold chemistry. *Molecular Physics* **107**, 99 (2009).
- [4] Balakrishnan, N. Perspective: Ultracold molecules and the dawn of cold controlled chemistry. *The Journal of Chemical Physics* **145**, 150901 (2016).
- [5] Zahzam, N., Vogt, T., Mudrich, M., Comparat, D. & Pillet, P. Atom-molecule collisions in an optically trapped gas. *Phys. Rev. Lett.* **96**, 023202 (2006).
- [6] Staanum, P., Kraft, S. D., Lange, J., Wester, R. & Weidemüller, M. Experimental investigation of ultracold atom-molecule collisions. *Phys. Rev. Lett.* **96**, 023201 (2006).
- [7] Hudson, E. R., Gilfoy, N. B., Kotochigova, S., Sage, J. M. & DeMille, D. Inelastic collisions of ultracold heteronuclear molecules in an optical trap. *Phys. Rev. Lett.* **100**, 203201 (2008).
- [8] Wang, T. T., Heo, M.-S., Rvachov, T. M., Cotta, D. A. & Ketterle, W. Deviation from universality in collisions of ultracold $^6\text{Li}_2$ molecules. *Phys. Rev. Lett.* **110**, 173203 (2013).
- [9] Ospelkaus, S. *et al.* Quantum-state controlled chemical reactions of ultracold potassium-rubidium molecules. *Science* **327**, 853 (2010).
- [10] Ni, K.-K. *et al.* Dipolar collisions of polar molecules in the quantum regime. *Nature* **464**, 1324 (2010).
- [11] de Miranda, M. H. G. *et al.* Controlling the quantum stereodynamics of ultracold bimolecular reactions. *Nat. phys.* **7**, 502 (2011).
- [12] Knoop, S. *et al.* Magnetically controlled exchange process in an ultracold atom-dimer mixture. *Phys. Rev. Lett.* **104**, 053201 (2010).
- [13] Lompe, T. *et al.* Atom-dimer scattering in a three-component fermi gas. *Phys. Rev. Lett.* **105**, 103201 (2010).
- [14] Rui, J. *et al.* Controlled state-to-state atom-exchange reaction in an ultracold atom-dimer mixture. *Nat. Phys.* **13**, 699 (2017).
- [15] Drews, B., Deiβ, M., Jachymski, K., Idziaszek, Z. & Denschlag, J. H. Inelastic collisions of ultracold triplet Rb_2 molecules in the rovibrational ground state. *Nat. Commun.* **8**, 14854 (2017).
- [16] Zhao, B., Glaetzle, A. W., Pupillo, G. & Zoller, P. Atomic Rydberg reservoirs for polar molecules. *Phys. Rev.*

- Lett.* **108**, 193007 (2012).
- [17] Carr, L. D., DeMille, D., Krems, R. V. & Ye, J. Cold and ultracold molecules: science, technology and applications. *New J. Phys.* **11**, 1367 (2009).
- [18] Moore, M. G. & Vardi, A. Bose-enhanced chemistry: Amplification of selectivity in the dissociation of molecular bose-einstein condensates. *Phys. Rev. Lett.* **88**, 160402 (2002).
- [19] Bauer, J., Salomon, C. & Demler, E. Realizing a Kondo-correlated state with ultracold atoms. *Phys. Rev. Lett.* **111**, 215304 (2013).
- [20] Nishida, Y. Su(3) orbital kondo effect with ultracold atoms. *Phys. Rev. Lett.* **111**, 135301 (2013).
- [21] Quémener, G. & Julienne, P. S. Ultracold molecules under control. *Chem. Rev.* **112**, 4949 (2012).
- [22] Herschbach, D. Molecular collisions, from warm to ultracold. *Faraday Discuss.* **142**, 9–23 (2009).
- [23] Tomza, M. Energetics and control of ultracold isotope-exchange reactions between heteronuclear dimers in external fields. *Phys. Rev. Lett.* **115**, 063201 (2015).
- [24] D’Incao, J. P. & Esry, B. D. Ultracold three-body collisions near overlapping feshbach resonances. *Phys. Rev. Lett.* **103**, 083202 (2009).
- [25] Wu, C.-H., Park, J. W., Ahmadi, P., Will, S. & Zwiernlein, M. W. Ultracold fermionic feshbach molecules of $^{23}\text{Na}^{40}\text{K}$. *Phys. Rev. Lett.* **109**, 085301 (2012).
- [26] Chin, C. & Julienne, P. S. Radio-frequency transitions on weakly bound ultracold molecules. *Phys. Rev. A* **71**, 012713 (2005).
- [27] Upadhyay, S. K. *Chemical Kinetics and Reaction Dynamics* (Springer & Anamaya Publishers New Delhi, 2006).
- [28] Braaten, E. & Hammer, H.-W. Universality in few-body systems with large scattering length. *Phys. Rep.* **428**, 259 (2006).
- [29] Braaten, E., Hammer, H. W., Kang, D. & Platter, L. Efimov physics in ^6Li atoms. *Phys. Rev. A* **81**, 013605 (2010).
- [30] Helfrich, K., Hammer, H.-W. & Petrov, D. S. Three-body problem in heteronuclear mixtures with resonant interspecies interaction. *Phys. Rev. A* **81**, 042715 (2010).

Supplementary Information

A. Feshbach resonance

The scattering length near the Feshbach resonance $\tilde{a}(B) = a_{\text{bg}}[1 - \Delta B/(B - B_0)]$ has been determined in Ref. [S1] by fitting the binding energies of the Feshbach molecules using the universal model. For the Feshbach resonance between A and B, we obtain $a_{\text{bg}} = -455 a_0$, $B_0 = 138.71$ G and $\Delta B = -34.60$ G. For the Feshbach resonance between A and C, we have $a_{\text{bg}} = 126 a_0$, $B_0 = 130.637$ G and $\Delta B = 4.0$ G. The binding energies of the Feshbach molecules are given by $E_{ij}^b = \hbar^2/2\mu_d a_{ij}^2$, where $a_{ij} = \tilde{a}_{ij}(B) - \bar{a}$, with $\bar{a} = 51 a_0$ being the mean scattering length. The scattering lengths and

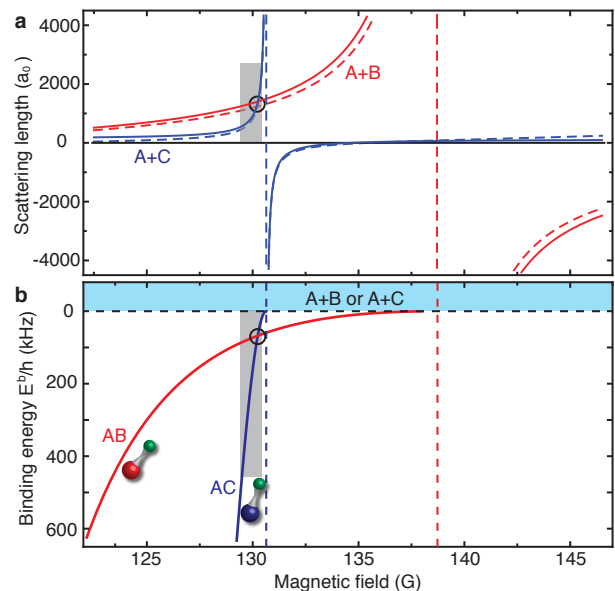


FIG. S1: **Overlapping Feshbach resonance.** **a.** The scattering lengths of the collision channels A + B (red) and A + C (blue). Solid lines represent the scattering lengths from the universal model. Dashed lines represent the results from the coupled-channel calculations. **b.** The binding energies of the weakly bound AB and AC Feshbach molecules obtained from the universal model, which predict the two curves to intersect at 130.24 G. The grey shaded region denotes the range of magnetic fields in which the current experiment is performed.

binding energies are shown in Fig. S1. Here a_{AB} and a_{AC} are the input parameters in the STM equations. From the binding energy curves, we obtain $E_{\text{AB}}^b = E_{\text{AC}}^b$ at $B = 130.24(1)$ G, which is about 10 mG smaller than $B_{tn} = 130.249(2)$ G which was determined from the direct measurement. Therefore, in the numerical calculations, the magnetic field is shifted by 10 mG to compare with the experiments.

B. Raman photoassociation and molecular bound-bound transition

In this work, we employ Raman photoassociation to form AC Feshbach molecules [S2]. We use two blue-detuned Raman light fields to couple the $|9/2, -1/2\rangle$ and C states with a single-photon detuning of $\Delta \approx 2\pi \times 251$ GHz, with respect to the D2 line transition of the ^{40}K atom, as shown in Fig. S2. The two Raman beams have a frequency difference of approximately $2\pi \times 37$ MHz at the magnetic fields of around 130 G. Thus, they can be simply created by using two acousto-optic modulators with the light field from a single laser. The width of each Raman beam is about 0.8 mm at the position of the atoms, and the power is 30 mW. The Raman Rabi frequency for the $|9/2, -1/2\rangle \rightarrow \text{C}$ transition is about $2\pi \times 90$ kHz.

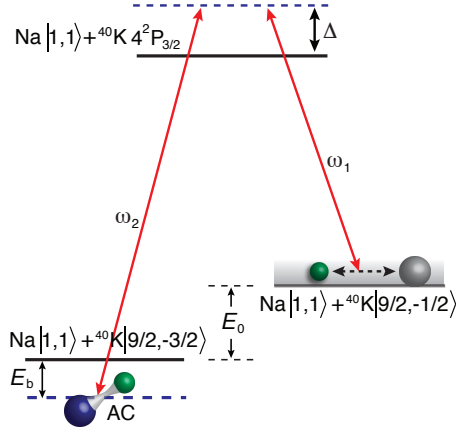


FIG. S2: **Raman photoassociation.** The atom mixture is initially prepared in the $A + |9/2, -1/2\rangle$ state. The AC molecule is formed by the Raman light. E_b denotes the binding energy of the AC molecules. E_0 denotes the free atomic transition frequency between the two spin states of K atoms.

To associate the AC molecules from the $A + |9/2, -1/2\rangle$ mixture, we use a 300- μs Gaussian pulse with a full width at half maximum (FWHM) duration of about 150 μs . Using a Gaussian pulse, the high Fourier side lobes can be efficiently suppressed, and thus the transfer of free atoms from the $|9/2, -1/2\rangle$ to the C state can be neglected. The Raman light fields have no influence on the active stabilization loop of the magnetic field, and thus it does not cause a shift of the magnetic field.

After creating the AC molecules, we determine the molecular bound-bound transition frequency $\nu_{AC \rightarrow AB}$ by measuring the molecule radio-frequency (rf) spectrum. This is achieved by first transferring the AC molecule to the AB molecule via a rf pulse, and then the AB molecules are detected by dissociating them into the $A + |9/2, -7/2\rangle$ state for imaging. Besides, we also measure the free atomic transition frequency $\nu_{C \rightarrow B}$ by measuring the rf spectrum between the C and B states. From these measurements, the reaction energy change $\Delta E = \nu_{AC \rightarrow AB} - \nu_{C \rightarrow B}$ can be accurately determined, and the results are shown in Fig. 1 in the main text. After determining the bound-bound transition frequency, the Rabi oscillation between the AB and AC molecule states is measured, and thus the duration of the π pulse is determined.

C. Remove the remaining A atoms and the AC molecule products

To demonstrate that the discrepancy between the time constants τ_{AB} and τ_B for the endothermic reaction and nearly thermoneutral reaction is caused by the reverse reaction, we remove the AC molecule products continuously during the reaction process by dissociating

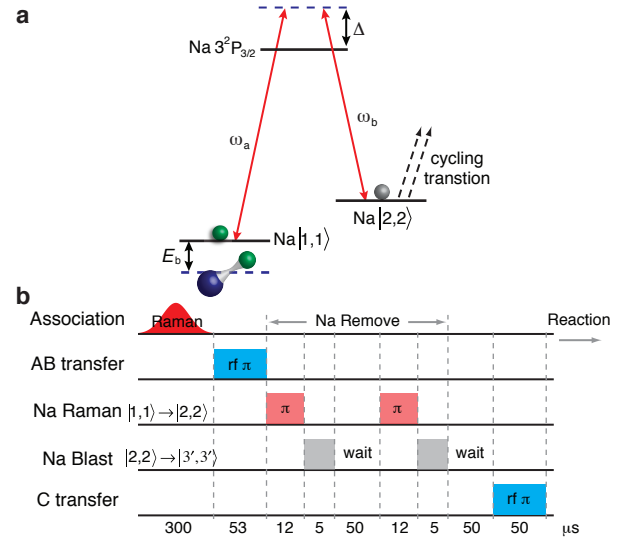


FIG. S3: **Removal of the remaining A atoms.** **a.** The energy levels of the two-photon Raman transition used for transferring the Na atoms from the A to the $|2, 2\rangle$ state. After the Raman transfer, the Na atoms in the $|2, 2\rangle$ state are resonantly blasted out of the optical trap by a light pulse resonant with the cycling transition. **b.** The time sequence of the preparation process including the removal of the remaining A atoms.

them into the $A + |9/2, -1/2\rangle$ state. However, the remaining A atoms and the residual $|9/2, -1/2\rangle$ atoms due to the imperfection of the π pulse may cause a competition between the dissociation and association process. Therefore, we first remove the A atoms after the AB molecules have been prepared. This is achieved as follows. We first transfer Na atoms from the A to the $|2, 2\rangle$ state using a blue-detuned Raman π pulse with a single-photon detuning of $\Delta \approx 2\pi \times 215$ GHz with respect to the D2 line of Na atom, and then blast them out of the optical trap by applying a light pulse resonantly coupling the $|2, 2\rangle \rightarrow |3', 3'\rangle$ cycling transition, as shown in Fig. S3a. The Raman fields for Na atoms have a width of about 1.1 mm at the position of the atoms, and each beam has a power of about 50 mW, which yields a Raman Rabi frequency of $2\pi \times 46$ kHz for the $A \rightarrow |2, 2\rangle$ transition. The Raman-Blast sequences are applied twice to completely remove the remaining A atoms. The time sequence including the removal of the A atoms is shown in Fig. S3b. The Raman-Blast process also causes small loss of the AB molecules. Typically, we still keep 90% of the AB molecules after removing the remaining A atoms.

Then we can remove the AC molecule products during the reaction process by continuously dissociating them into the $A + |9/2, -1/2\rangle$ state. This is achieved by using the Raman light coupling the $|9/2, -1/2\rangle$ and the C states, which is also used to associate the AC molecules. For the dissociation, the two-photon detuning is tuned to be 220–320 kHz above the bound-free transition, and the powers of both beams are reduced to obtain half the peak

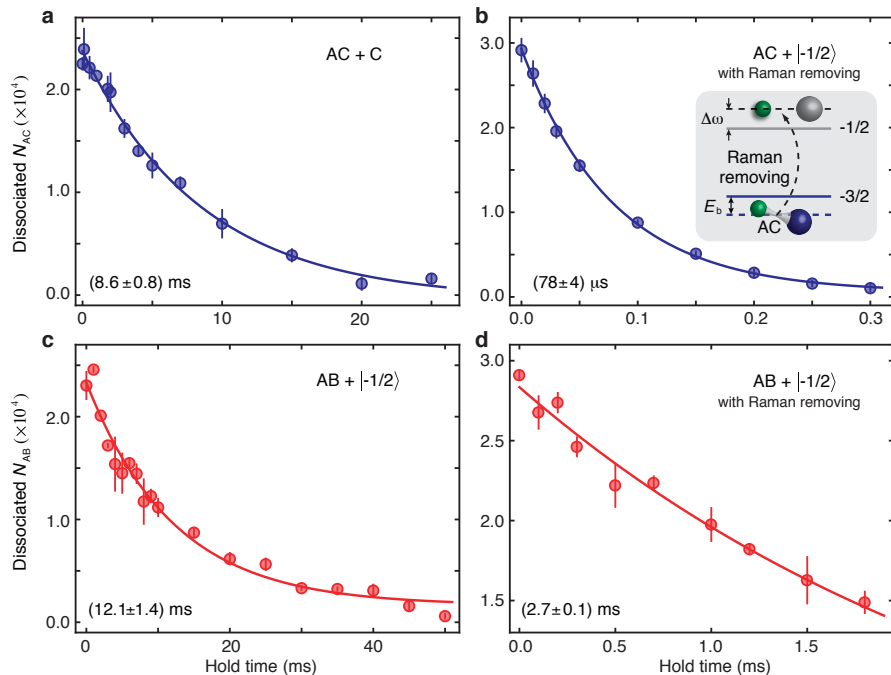


FIG. S4: **Lifetime of the molecules under different conditions.** The measurements are taken after removing the remaining A atoms at 130.26 G. **a** and **b**. The lifetime of the AC molecules without and with the Raman removing fields, respectively. The two-photon frequency is tuned to be about 220 kHz above the bound-free transition frequency. The AC molecules are detected by first transferring them to the AB state and then dissociating them into the $A + |9/2, -7/2\rangle$ state. **c** and **d**. The lifetime of the AB molecules without and with the Raman removing fields, respectively. Error bars represent ± 1 s.d.

intensity as was used in the association process. This Raman dissociation light reduces the lifetime of the AC molecules to around $80 \mu\text{s}$, as is shown in Fig. S4b, and thus the AC molecules can be quickly eliminated. We checked that the Raman removing pulse has negligible effects on the C atoms. The Raman removing pulse also affects the lifetime of the AB molecules. However, the AB molecule still has a lifetime of about 2.7 ms under the Raman removing fields, as is shown in Fig. S4d, which is long enough for the study of the reaction dynamics.

We also compare the time evolutions when only removing the remaining A atoms and the time evolutions when both the remaining A atoms and the AC molecules are removed. After removing the A atoms, the dominant atoms in the mixture are the C atoms. The AC molecule has a long lifetime of about 8 ms when coexisting with the C atoms, as shown in Fig. S4a. In this case, the effects of the reverse reaction may also be observed on a long time scale. As shown in Fig. S5, when only the A atoms are removed, we observe a long-term decay for the B atom products. However, this long-term decay disappears when the AC products are continuously removed during the reaction process. Therefore, we attribute this long-term decay to the influence of the reverse reaction.

Besides, we also measure the influence of the Raman removing light on the molecular and atomic transition frequencies. Our measurements show that the atomic transition frequency $\nu_{C \rightarrow B}$ is shifted by about +0.3 kHz,

whereas the molecular bound-bound transition frequency $\nu_{AC \rightarrow AB}$ is shifted by about -3.4 kHz. The energy change $\Delta E = \nu_{AC \rightarrow AB} - \nu_{C \rightarrow B}$ under the Raman removing fields is plotted in Fig. S6. The polynomial fitting shows the magnetic field of zero energy change is shifted to 130.258(2) G under the Raman removing fields.

D. Reaction dynamics

Taking into account the reverse reaction, the time evolution of the AB reactant and B product may be described by

$$\dot{N}_{AB} = -\gamma_{AB}N_{AB} + k_{re}N_{AC}N_B, \quad (3)$$

$$\dot{N}_B = \beta_r \bar{n}_C N_{AB} - k_{re}N_{AC}N_B, \quad (4)$$

where the first and second term of the right side account for the forward and reverse reaction respectively. The time evolution of the AC molecule may be written in a similar form as the AB molecule. Since the time evolution of the AC molecule is difficult to detect, its equation is not shown. Here the overall loss rate of N_{AB} is $\gamma_{AB} = \beta_A \bar{n}_A + \beta_C \bar{n}_C + \beta_r \bar{n}_C$, with \bar{n}_A and \bar{n}_C the mean densities of the A and C atoms, respectively. The first term accounts for the loss due to inelastic collisions with the remaining A atoms, with β_A the loss rate coefficient. When the A atoms are removed, this term can

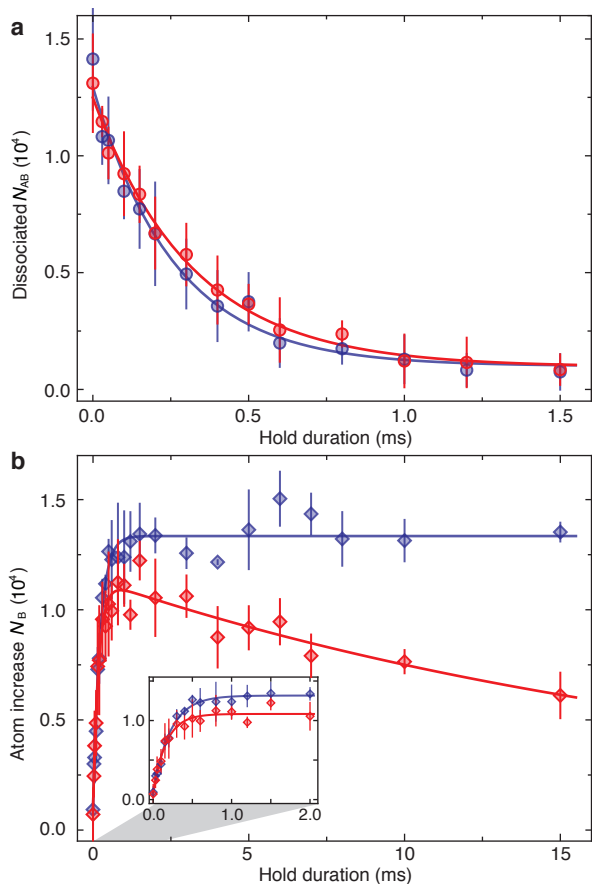


FIG. S5: **Time evolution after removing the remaining A atoms.** The red (blue) data points represent the time evolution without (with) applying the Raman removing light at 130.26 G. **a.** The time evolution of the AB reactants. The time constants are measured to be $\tau_{AB} = 0.319(21)$ ms (red) and $\tau_{AB} = 0.262(28)$ ms (blue), respectively. **b.** The time evolutions of the B products, which are fitted with the model, $N_B(t) = N_B^0(e^{-t/\tau_2} - e^{-t/\tau_1})$. The fitting gives $\tau_1 = 0.184(24)$ ms and $\tau_2 = 21(4)$ ms (red), and $\tau_1 = 0.220(18)$ ms and $\tau_2 = +\infty$ (blue). (**Inset**). The short term evolution of the B products. The simple exponential fitting gives a time constant of $\tau_B = 0.166(22)$ ms (red), and $\tau_B = 0.220(18)$ ms (blue). Error bars represent ± 1 s.d.

be neglected. The other two terms describe the losses due to collisions with the atom reactant C, which include the desired reactive collision with a reaction rate coefficient of β_r , and the losses due to reactions in other channels and vibrational relaxations with an overall loss rate of β_C . The collisions between the AB molecules are neglected since the Feshbach molecules are fermionic molecules. We have assumed \bar{n}_A and \bar{n}_C are constants since the number of molecules is about one order of magnitude smaller than that of the atoms. The reverse reaction is caused by the reactive collisions between the AC molecule and B atom products with k_{re} the reverse reaction rate.

In our experiment, the time evolutions of $N_{AB}(t)$ and $N_B(t)$ are measured. To extract the reaction rate

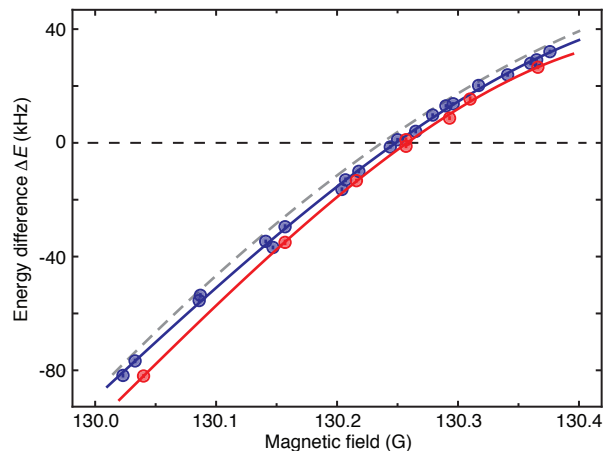


FIG. S6: **Influence on the energy change of the Raman removing fields.** The red points represent the measured energy change under the Raman removing fields. The blue points represent the energy change in the main text. The solid lines are polynomial fitting to the measured values, which shows the zero-energy-change magnetic field is shifted by 9 mG under the Raman fields. The grey dashed line is the energy change calculated from the universal binding energy curves. Error bars inside the circles represent ± 1 s.d.

coefficient, we use

$$\beta_r = \frac{\dot{N}_B(0)}{\bar{n}_C N_{AB}(0)}. \quad (5)$$

This is reasonable as we start from the AB + C mixture and thus at $t = 0$ the number of products N_{AC} and N_B can be neglected. The exact form of $N_{AB}(t)$ and $N_B(t)$ are difficult to know. Therefore, we assume they may be approximated by exponentials and use exponentials to fit the data points. The reaction rate coefficients are extracted with $N_{AB}(0)$ and $\dot{N}_B(0)$ obtained from the fitting curves. Note that when the reverse reaction is suppressed or can be neglected, the analytic solutions of $N_{AB}(t)$ and $N_B(t)$ are exponentials, and thus reaction rate coefficients obtained from Eq. (5) are exact.

The initial molecule number has to be corrected by taking into account the finite rf dissociation rate [S1], since the reaction is fast. The finite π -pulse transfer efficiency of the K atoms from the B to $|9/2, -7/2\rangle$ states also needs to be included, which is about 90% with the Na atoms, and 95% without the Na atoms. Finally, all uncertainties of the parameters are included to give the uncertainty in the reaction rate coefficients.

E. STM equations

The scattering amplitudes satisfy the STM equations

$$\begin{aligned}
 t_{ii}(k, p, E) &= \frac{m_A}{\pi\mu_d} \sqrt{\frac{a_{AC}}{a_{AB}}} \int^\Lambda dq \frac{q}{2k} K(k, q, E) \\
 &\quad \times D_{AC}(q, E) t_{fi}(q, p, E) \\
 t_{fi}(k, p, E) &= \frac{2\pi\hbar^4}{\mu_d^2 \sqrt{a_{AB}a_{AC}}} \frac{m_A}{2pk} K(k, p, E) \\
 &\quad + \frac{m_A}{\pi\mu_d} \sqrt{\frac{a_{AB}}{a_{AC}}} \int^\Lambda dq \frac{q}{2k} K(k, q, E) \\
 &\quad \times D_{AB}(q, E) t_{ii}(q, p, E)
 \end{aligned} \tag{6}$$

where

$$\begin{aligned}
 K(k, p, E) &= \log \frac{2\mu_d E - p^2 - k^2 + 2\mu_d pk/m_A}{2\mu_d E - p^2 - k^2 - 2\mu_d pk/m_A} \\
 D_{jl}(q, E) &= \left[-\frac{\hbar}{a_{jl}} + \sqrt{-2\mu_d \left(E - \frac{q^2}{2\mu_{ad}} \right)} \right]^{-1}.
 \end{aligned}$$

We denote the input channel AB + C by channel i and the reaction channel AC + B by channel f , and thus $t_{ii}(k, p, E)$ is the elastic scattering amplitude, or in other words, the back-reflection amplitude of scattering into the input channel, and $t_{fi}(k, p, E)$ is the reactive scattering amplitude, with p and k being the relative momentum of the incoming and outgoing atom-dimer pairs and E the total energy, $\mu_d = m_A m_B / (m_A + m_B)$ is the reduced mass, and $\mu_{ad} = m_A (m_A + m_B) / (2m_A + m_B)$ is the reduced mass of atom and dimer. In the integral equations, the only input parameters are the scattering lengths a_{AB} and a_{AC} , which have been given in Sec. A in the Supplementary Information, and the unknown three-body parameter Λ , which will be determined by comparing the reaction rates. Since the magnetic field window in the experiment is narrow, we assume Λ is a constant.

We numerically solve the STM integral equations to calculate the on-shell reaction amplitudes $t_{fi}(k_f, p_i, E)$ with $E = \hbar^2 k_f^2 / 2\mu_d - E_{AC}^b = \hbar^2 p_i^2 / 2\mu_d - E_{AB}^b$ using the method introduced in Ref. [S3, S4]. The incident relative momentum is calculated for $p_{\min} \leq p_i \leq p_{\max}$, where $p_{\min} = 0$ for the exothermic reactions and $p_{\min} = \sqrt{2\mu_d |\Delta E|}$ for the endothermic reactions, and $p_{\max} = \sqrt{2\mu_d E_{AB}^b}$, i.e., we only consider the collisional kinetic energy smaller than the binding energy of the AB molecule. This is a good approximation since in our experiment we have $E_{AB}^b > 4k_B T$. The total reaction cross section is given by $\sigma_r(p_i) = (8\pi^3/h^4) \mu_{ad}^2 (k_f/p_i) |t_{fi}(k_f, p_i, E)|^2$. The reaction rate coefficient is thus calculated by $\beta_r = \int v \sigma_r(v) f(v) dv$ where we have $v = p/\mu_{ad}$ and $f(v) = 4\pi v^2 [\mu_{ad}/(2\pi k_B T)]^{3/2} \exp[-(\mu_{ad} v^2)/(2k_B T)]$ is the Maxwell-Boltzmann distribution. In the calculation, the temperature is assumed to be 700 nK, and the magnetic field has been shifted 10 mG so that the overlapping magnetic field obtained from the universal binding energy curves is consistent with the direct measurement.

The calculated rate coefficients are compared with the experiment for the magnetic fields between 129.44 G to 130.38 G, where the data points between 129.44 G and 129.91 G are obtained from our previous work. The reaction rate at 130.03 G is also measured in our previous work [S1]. However, due to the suppression of the bound-free Franck-Condon coefficients, the number of the AB molecule that can be formed from the A+C mixture is only about 5000. In comparison, using the indirect method in this work, 1.5×10^4 AB molecules can be formed. Therefore, at 130.03 G, the reaction rate measured in this work has much better signal-to-noise ratio and thus is used in the fitting. For the magnetic fields larger than 130.03 G, the reaction rates can only be measured using the current method.

-
- [S1] Rui, J. *et al.* Controlled state-to-state atom-exchange reaction in an ultracold atom-dimer mixture. *Nat. Phys.* **13**, 699 (2017).
[S2] Fu, Z. *et al.* Production of feshbach molecules induced by spin-orbit coupling in fermi gases. *Nat. phys.* **10**, 110 (2014).
[S3] Braaten, E., Hammer, H.-W., Kang, D. & Platter,

- L. Three-body recombination of ^6Li atoms with large negative scattering lengths. *Phys. Rev. Lett.* **103**, 073202 (2009).
[S4] Helfrich, K., Hammer, H.-W. & Petrov, D. S. Three-body problem in heteronuclear mixtures with resonant interspecies interaction. *Phys. Rev. A* **81**, 042715 (2010).